



Effect of tantalum contents on transformation temperatures, thermal behaviors and microstructure of CuAlTa HTSMAs

E. Ercan¹ · F. Dagdelen² · I. N. Qader^{2,3}

Received: 8 January 2019 / Accepted: 25 May 2019 / Published online: 4 June 2019
© Akadémiai Kiadó, Budapest, Hungary 2019

Abstract

In this study, CuAl_{13-x}Ta_x (% mass $x = 1; 1.5; 2; 2.5$) shape-memory alloys were produced through arc-melting method. Phase transformation temperatures were investigated by using differential scanning calorimetry (DSC) and thermogravimetric analysis. Microstructures were examined with the aid of optical microscopy, scanning electron microscopy–energy-dispersive X-ray (SEM–EDX) and X-ray diffraction (XRD). The ratios of electron per atom (*ela*) for CuAl_{13-x}Ta₁, CuAl_{13-x}Ta_{1.5}, CuAl_{13-x}Ta₂ and CuAl_{13-x}Ta_{2.5} were calculated as 1.52, 1.51, 1.50 and 1.49, respectively. DSC results showed that CuAlTa alloys belong to high-temperature shape-memory alloys. Also, it was identified that these alloys demonstrate $2H(\gamma'_1) \rightarrow DO_3(\beta_1) \rightarrow 18R(\beta'_1)$ phase transformation. It was observed that both phase transformation temperature and oxidation sensitivity of the samples decreased with the increase in the amount of Ta. In the XRD analysis of CuAlTa HTSMA alloys, some phases were observed, including γ' , β' , Cu₉Al₄, CuAl and Ta₂Al₃. These phases were supported by SEM–EDX results. The micro-hardness values of the alloys were increased by increasing Ta content.

Keywords Martensitic phase · Microstructure · Oxidation sensitivity · Shape-memory alloy

Introduction

Due to the great contribution to developing smart technology, shape-memory alloys have become popular for the last few decades. These materials are used widely in various fields, such as biomedical, aerospace, nuclear industry and automobile industry. The use of alloys in different applications has rapidly accelerated the developments in research area [1–3]. The use of implants, prostheses, sensors, actuators, pipe couplings, noise reduction is some of these applications. Shape-memory alloys are divided into three main families, including iron-based [4], copper-based [5] and nickel–titanium–X materials [6, 7]. Ni–Ti alloys exhibit better shape-memory properties and corrosion

resistance than Cu-based alloys. However, the production of NiTi alloys is more expensive than Cu-based alloys and is more fragile and difficult to process. In addition, Cu-based alloys exhibit shape-memory effect (SME) and super-elasticity (SE) better than Fe-based alloys [8–10]. For these reasons, Cu-based shape-memory alloys are widely used nowadays. Cu-based alloys are usually derived from three different binary alloy systems: Cu–Zn, Cu–Al and Cu–Sn [11]. The martensitic transformation in Cu–Sn alloys is not ideal for thermoelastic [12]. The materials formed by adding the third element into Cu–Zn (Al, Si, Sn) and Cu–Al (Ni, Be, Mn) alloys show shape memory and also exhibit martensitic transformation in a wide range of temperatures [13–18]. In particular, in this sense, it is important that HTSMAs are widely used in fields such as nuclear power plants, space industry and engineering applications [19–21].

Today, some alloying systems such as Cu–Al–Ni, Cu–Al–Mn, Cu–Al–Fe and Cu–Al–Ag have been investigated [16–18, 22]. Martensitic transformation temperatures, thermal stability and mechanical properties can be adjusted by adding the third element to the Cu–Al-based alloys. However, some problems such as low thermal stability,

✉ F. Dagdelen
fdagdelen@firat.edu.tr

¹ Department of Physics, Science Faculty, Bitlis Eren University, Bitlis, Turkey

² Department of Physics, Science Faculty, Firat University, Elazig, Turkey

³ Department of Physics, College of Science, University of Raparin, Sulaimaniyah, Iraq

microstructure and practical application still remain in this alloy system. For example, Cu–Al–Ni shape-memory alloys have better thermal stability and high operating temperatures, but their practical applications are limited by poor process ability. On the other hand, although Cu–Al–Mn shape-memory alloys have good ductility and workability, their operating temperatures are low [18]. The aforementioned properties are directly affected on the thermo-elastic martensitic transformations of these materials, which depend on the martensitic structure.

The martensitic structure of Cu–Al-based alloys is rather complicated than Ni–Ti alloys. Due to the composition of the alloy in Cu–Al-based alloys, the existence of different martensitic structures, such as α' , β' and γ' , has made working in these alloys even more interesting [15, 23–25]. These alloys' two ordering mechanisms are possible in the presence of Cu₃Al composition. The first one is the transformation from disordered bcc-type (A2) structure to the CsCl-type (B2) structure at 700 °C, while the second one is the ordering transformation from B2 structure to DO₃ structure at 570 °C [26]. Also, the martensitic transformation temperature of Cu–Al-based alloys is generally stable at high temperatures. For this, the disordered β phase of Cu–Al-based alloys is heated at appropriate temperatures and then ordered is quenched [18]. At the end of this process, the precipitates of the α -phase pass the suppressed state. There are some differences in crystal structure between the α -phase and the β -phase, which are important for thermal activation of the driving force [25].

With the help of the third elements added to Cu–Al-based alloys, some characteristics [27] such as microhardness, phase transformation kinetics, oxidation parameters and microstructure can be modified. The purpose of this study is to produce HTSMAs by adding different percentages of Ta elements into Cu–Al-based alloys. And also to examine the oxidation parameters, phases that may occur at high temperature, martensitic phase transformations, and microstructure of the produced alloys.

Experimental procedure

The produced Cu–Al–Ta alloys with four different chemical compositions and their corresponding electron concentration values are listed in Table 1. The samples were melted in an arc furnace under argon atmosphere and cast into 20 g of ingots, by using highly pure (99% copper, 99.5% aluminum and 99.9% tantalum) elements. The prepared samples were homogenized at 900 °C for 24 h. Firstly, the alloys were cut into cubes approximately $2 \times 2 \times 2$ mm for DSC and TG/DTA measurements. In order to neutralize the surface roughness, which appeared

Table 1 Atomic, mass and e/a rates of Cu–Al–Ta alloys

Samp.	mass%			at%			e/a
	Cu	Al	Ta	Cu	Al	Ta	
CAT1	86	13	1	73.52	26.18	0.30	1.52
CAT2	86	12.5	1.5	74.15	25.40	0.45	1.51
CAT3	86	12	2	74.80	24.60	0.60	1.50
CAT4	86	11.5	2.5	75.47	23.76	0.77	1.49

during cutting process, it was heated again at 900 °C for 30 min and cooled down through saline ice water. The heating/cooling rates were selected as 20 °C min⁻¹ for thermal measurement. XRD measurement of the alloys was measured at room temperature. For surface morphology investigation, the samples were polished; after that, they were washed with alcohol and dried and then etched in 10 mL HCl + 48 mL methanol + 2.5 g FeCl₃–H₂O for 5 s. Etched samples were photographed using a Nikon MA 100 optical microscope (OM). The micro-hardness measurements of the samples were measured using QNESS 10 brand devices. Finally, the chemical compositions of the phase region and precipitates in alloys were determined by a scanning electron microscope/energy-dispersive X-ray spectrometer (SEM/EDX) (Bruker-125).

Results and discussion

It is crucial to define phase transformation temperatures of SMAs according to A_s : austenite start, A_f : austenite finish, M_s : martensite start, M_f : martensite finish. In order to determine these temperatures, DSC measurements of alloys were done for alloys that were quenched in ice water. Heating and cooling rates were chosen as 20 °C min⁻¹. The results are given in Fig. 1 and Table 2. These results

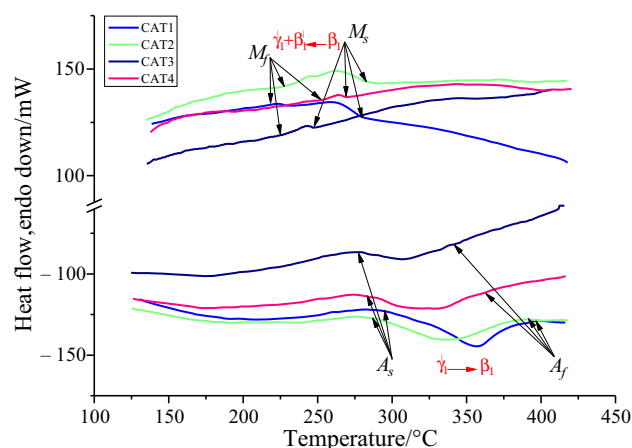


Fig. 1 DSC curves of CuAlTa alloys

show that the CuAlTa alloys exhibit HTSMAs. Also, by increasing the amount of Ta in CuAl-based HTSMAs, the phase transformation temperatures are reduced. Moreover, the required enthalpy energy for phase transformation was calculated such that from the austenite phase to the martensite phase, $\Delta H_{CuAl13Ta1}^{M \rightarrow A} = 2.51 \text{ J g}^{-1}$, $\Delta H_{CuAl13Ta1.5}^{M \rightarrow A} = 2.10 \text{ J g}^{-1}$, $\Delta H_{CuAl13Ta2}^{M \rightarrow A} = 1.18 \text{ J g}^{-1}$ and $\Delta H_{CuAl13Ta2.5}^{M \rightarrow A} = 1.97 \text{ J g}^{-1}$; however, for the reverse transformation, it was $\Delta H_{CuAl13Ta1}^{M \rightarrow A} = -0.65 \text{ J g}^{-1}$, $\Delta H_{CuAl13Ta1.5}^{M \rightarrow A} = -0.65 \text{ J g}^{-1}$, $\Delta H_{CuAl13Ta2}^{M \rightarrow A} = -0.05 \text{ J g}^{-1}$ and $\Delta H_{CuAl13Ta2.5}^{M \rightarrow A} = -0.02 \text{ J g}^{-1}$.

The equilibrium temperature (T_0) and the entropy (ΔS) values were calculated using Eqs. (1) and (2), respectively [28–30]:

$$T_0 = \frac{A_f + M_s}{2} \tag{1}$$

$$\Delta S = \frac{\Delta H}{T_0} = \frac{1/2(\Delta H^{A \rightarrow M} + \Delta H^{M \rightarrow A})}{T_0} \tag{2}$$

Entropy values of the alloys are given in Table 2. These results show that phase transformation enthalpies reduced with increasing Ta rate in CuAlTa alloys. From literature review [26, 31], it is observed that the entropy value was decreased by adding Ta element into the CuAl-based alloy. This can be explained such that the absorbed and released energy in martensitic transformation is decreased when added to the CuAl-based. This change in energy leads to a decrease in entropy values. Additionally, Cu–Al alloys, containing 9–14 (mass%) Al, exhibit martensitic transformation, which is (the β (bcc) phase undergoes the transformations) if subjected to rapid cooling from high temperature. During quenching process for the alloys that contain more than $\sim 11\%$ Al, the β phase transforms firstly to the β_1 phase (DO_3) and then martensitically transforms to either β'_1 , $\beta'_1 + \gamma'$ or γ' [32]. It is seen that the alloys provide HTSMAs characteristics due to their transformation in the range of 220–390 °C. This characteristic can be adjusted by the addition of the Ta element to the CuAl-based alloy. As a matter of fact, when the phase diagram of CuAl alloy is examined, it is seen that Cu/Al ratio is increased and β region to γ zone is approached [33]. With constant Cu and decreasing Al/Ta chemical concentration ratio, the alloy approaches the critical γ region. In

Table 2 Peak temperatures of CuAlTa alloys

Samp.	$P_1/^\circ\text{C}$	$P_2/^\circ\text{C}$	$P_3/^\circ\text{C}$	$P_4/^\circ\text{C}$	$P_5/^\circ\text{C}$
CAT1	294	472	527	540	577
CAT2	292	448	528	540	577
CAT3	297	435	529	556	577
CAT4	284	415	–	–	565

this case, it causes change of martensitic transformation required for shape-memory alloys. In addition, the amount and properties of the third element added to Cu–Al-based alloys are important. Prashantha et al. [34] added Be element to CuAl-based alloy, and they observed that the transformation temperature was between -60 and -20 °C. As shown in Fig. 1, many thermodynamic parameters such as shape-memory effect (SME), transformation temperatures [$\gamma' \rightarrow \beta_1 (A_s \rightarrow A_f)$ and $\beta_1 \rightarrow \beta'_1 + \gamma'_1 (M_s \rightarrow M_f)$], hysteresis ($A_f - M_s$), equilibrium temperature (T_0), enthalpy (ΔH) and entropy changes (ΔS) were affected by changing Ta addition. In Fig. 2, the transformation and equilibrium temperatures of the alloys were compared. While the ratio of Al/Ta element was decreased, the hysteresis range expanded. It is known that high transformation temperature and wide hysteresis range are needed in some special areas such as pipe joining, space and aerospace and heating engine. Apart from the changing composition, some other parameters can affect the martensitic transformations such as homogenization, precipitates and impurities.

Figure 3 shows the obtained DTA curves for CuAlTa alloys with a heating rate of $20 \text{ }^\circ\text{C min}^{-1}$. Five thermal events were detected: two exothermic peaks (E_1 and E_4) and three endothermic peaks (E_2 , E_3 and E_5). The α (Cu-rich) phase, formed at point P_1 , is known as the precipitate reaction generated from the martensitic phase, which is produced through quenching process. α (Cu-rich) phase is the solid solution of aluminum in copper that can usually transform into α_2 -superstructure below 340 °C. These transformations are recyclable during reheating, and thus the transformation order has general form: $\alpha_2 \leftrightarrow \gamma_2 \leftrightarrow \alpha + \gamma_2 \leftrightarrow \beta$. A martensitic transformation take places from β -phase by quenching the alloy into ice water. But before an ordering, β_1 -phase occurs. These

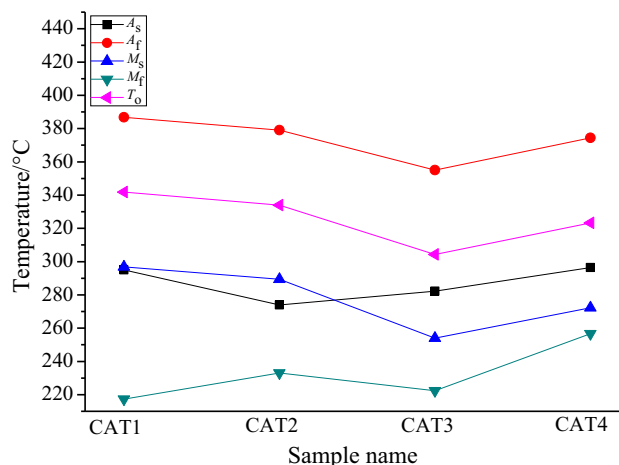


Fig. 2 Changes in transformation temperatures and T_0 of CuAlTa alloys

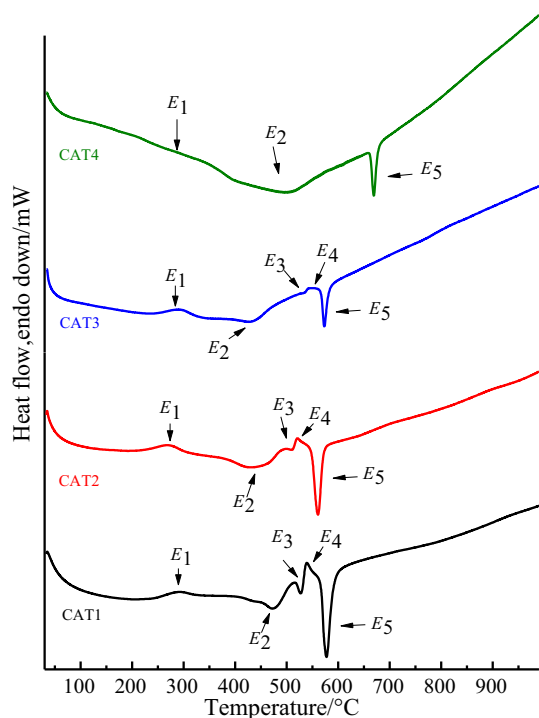


Fig. 3 DTA curves of CuAlTa alloys between 40 and 1000 °C

transformations are recyclable by rapid heating, and their sequences are in the form of $\beta \rightarrow \beta_1 \rightarrow \beta'_1$; also they are associated with SME in copper-rich CuAl alloys [35]. In addition, the second heating peak (P_2) is the martensite decomposition peak, which occurs in two successive reactions. The first is the $\beta_1 \rightarrow [\alpha(\text{CuAl}) + \gamma_2(\text{Cu}_9\text{Al}_4)]$ peritectoid reaction phase, which represents the reverse martensitic reaction and $\beta'_1 \rightarrow \beta_1$ transition, while the second is the decomposition of the β_1 phase. It is known that β and β_1 phase decomposition cannot be completely prevented. For this reason, the third endothermic peak P_3 is known as $\beta_1 \rightarrow \beta$ transition [35]. P_4 peak is an exothermic phase; the previous $\alpha(\text{Cu})$ -rich phase from the eutectoid reaction represents the precipitate reaction. This reaction is associated with the γ_2 -phase precipitation reaction. It provides the formation of $\alpha(\text{Cu})$ -rich solid solution by decreasing Al concentration in the matrix. P_5 exothermic peak was found to be related to $\alpha + \gamma_2 \leftrightarrow \beta + \gamma_2$ eutectoid reaction. It is known that this eutectic temperature is approximately at 567 ± 2 °C in $\alpha(\text{Cu})$ -rich alloys [35]. In addition, at this temperature, the sluggishness of the eutectoid reaction causes the β phase to be metastable. Table 2 gives the peak temperature values of the samples. When the peaks and the temperatures of these peaks are examined, it is obtained that the temperature of $\alpha(\text{Cu})$ -rich phase is reduced in the samples by decreasing the Al/Ta ratio. The $\alpha(\text{Cu})$ -rich phase (E_1), which is produced from the martensitic phase, is considerably reduced in the CAT4

sample. This decrease was also observed in the DSC peak. At E_2 peak, the formation temperature of the peritectoid reaction phase and $\beta'_1 \rightarrow \beta_1$ transition was decreased from 475 to 415 °C. In spite of this decrease, the increased amount of Ta element caused the E_2 phase reaction peak to be formed more widely. The E_3 peak representing the $\beta_1 \rightarrow \beta$ transition from the β_1 phase occurred at the same temperatures. However, in the CAT4 sample, when the E_2 peak was splayed in a wider temperature range, the β - and β_1 -phase decomposition was completely realized, so that the E_3 peak was not observed. Because the $\alpha(\text{Cu})$ -rich solid solution (E_1) was quite small in the CAT4 sample, the E_4 peak represents the $\alpha(\text{Cu})$ -rich phase precipitate which was not observed prior to the eutectic reaction. The E_5 peak was observed in all samples. However, in the CAT4 sample, the E_5 (eutectoid peak) temperature was observed at 565 °C, which is decreased by approximately 10 °C.

The TG mass gain curves were plotted for 40–1000 °C in air atmosphere, and the results are shown in Fig. 4. From Fig. 4, it is noticed that during oxidation, an irregularity can be seen up to 600 °C in the mass gain. After 600 °C, this irregular behavior is replaced by a constant increase. In addition, Fig. 3 shows the reason for the irregularity of the mass gain in the DTA curves. It is found that for the range of 260–680 °C, the precipitation, decomposition and the formation of martensitic phases, in all samples, are due to changes in the mass gain. Decreasing the irregularity in the mass gain between 700 and 1000 °C and increasing the amount of oxidation are important for determining the oxidation temperatures. Thus, the oxidation temperatures were chosen as 700 °C, 800 °C, 900 °C and 1000 °C. The oxidation constant rate (k_p) can be described by following relationship [36]:

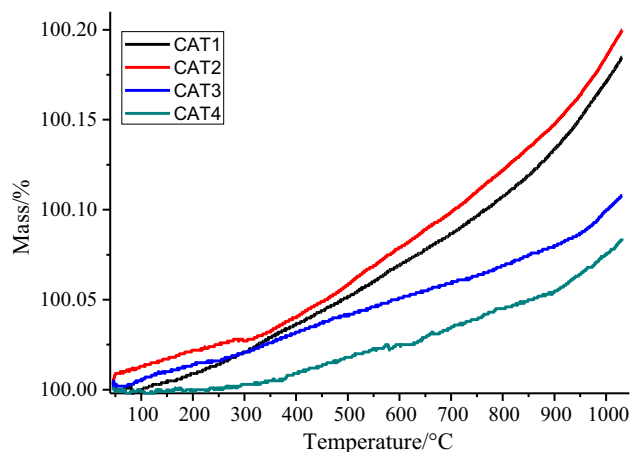
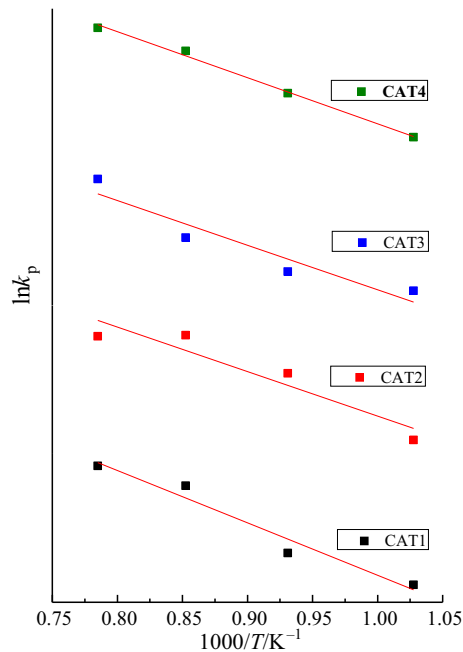


Fig. 4 Non-isothermal TG/DTA measurement of CuAlTa alloys 40–1000 °C in air atmosphere

Table 3 Transformation temperatures, enthalpy, entropy and activation energy for oxidation change value of CuAlTa alloys

Samp.	$A_s/^\circ\text{C}$	$A_f/^\circ\text{C}$	$M_s/^\circ\text{C}$	$M_f/^\circ\text{C}$	$T_o/^\circ\text{C}$	$A_f - M_s/^\circ\text{C}$	$\Delta H_{\text{cool}}/ \text{J g}^{-1}$	$\Delta H_{\text{heat}}/ \text{J g}^{-1}$	$\Delta S_{\text{cool}}/ \text{mJ g}^{-1} \text{ }^\circ\text{C}^{-1}$	$\Delta S_{\text{heat}}/ \text{mJ g}^{-1} \text{ }^\circ\text{C}^{-1}$	$E_o/ \text{kJ mol}^{-1}$
CAT1	295	386.8	296.8	217.3	341.8	90	-0.65	2.51	-1.90×10^{-3}	7.34×10^{-3}	51.38
CAT2	273.9	379.1	289.4	233.1	334	89.7	-0.65	2.10	-1.94×10^{-3}	6.28×10^{-3}	74.81
CAT3	282.2	355	254	222.3	304.3	101	-0.05	1.18	-0.16×10^{-3}	3.87×10^{-3}	100.1
CAT4	296.4	374.4	272.3	256.6	323.3	102.1	-0.02	1.97	-0.06×10^{-3}	6.09×10^{-3}	90.61

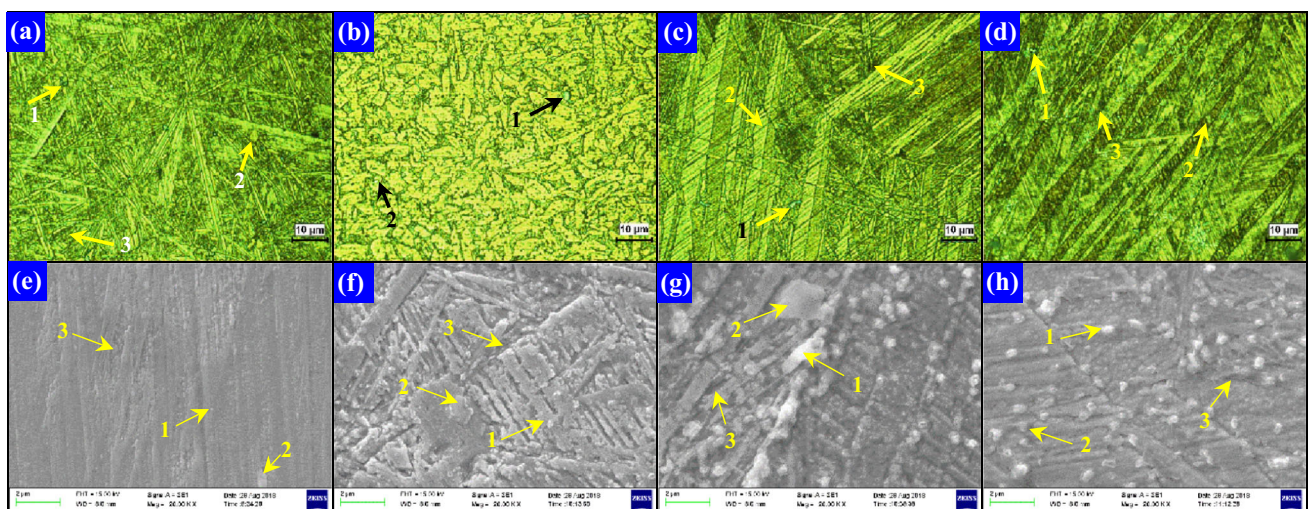
**Fig. 5** Arrhenius' curves for parabolic oxidation constant (k_p) in a temperature range of 700–1000 °C

$$\left(\frac{\Delta W}{A}\right)^2 = k_p t \quad (3)$$

where $(\Delta W/A)$ is the mass gain per unit area of a sample and t is the oxidation time. Thus, k_p can be calculated from the slope of linear regression line of $(\Delta W/A)^2$ versus t plot. According to k_p values of samples and temperature, the oxidation activation energy can be calculated by the following equation [36]:

$$k_p = k_0 \exp\left(-\frac{E_0}{RT}\right) \quad (4)$$

In light of the obtained results, activation energy for oxidation (E_o) is calculated and given in Table 3. In the oxidation process of CuAlTa alloy, the elements Al, Ta, Cu tend to give electrons, while the O element tends to receive electrons. For this reason, Cu, Al and Ta elements in the CuAlTa alloy react with oxygen to form Al_2O_3 , Ta_2O_5 and Cu_2O compounds [37]. The atomic radius of Ta is greater than the Al element. However, the ionization energy of Al is less than the Ta element. In this case, the activation energy for oxidation is increased by decreasing the Al/Ta ratio. However, as it can be seen in the DTA curve, the



where 1: $\text{Ta}_2(\text{Al}_2\text{Cu})_3$; 2: $\text{Cu}(\text{Al}_2\text{Ta})$; 3: $\gamma_1(\text{Cu}_2\text{Al}_4)$

Fig. 6 Optical micrographs (a–d) and SEM images (e–h) of CuAlTa alloys

Table 4 Result of EDX analyses for CuAlTa alloys

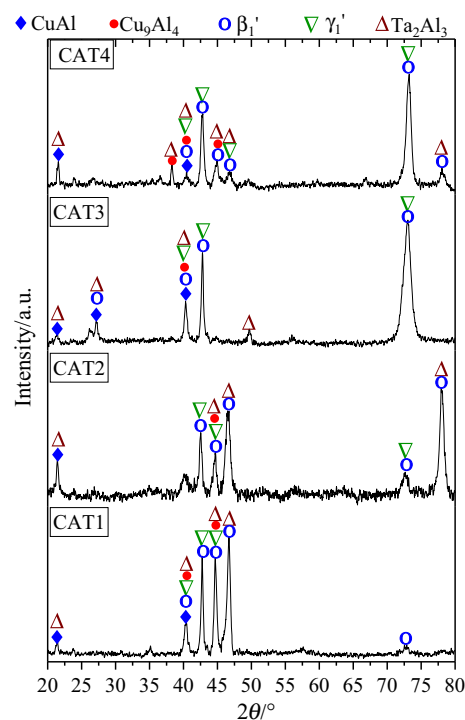
	Martensite			γ_1 (Cu ₉ Al ₄) phase			Cu(Al, Ta)			Ta ₂ (Al, Cu) ₃		
	Cu	Al	Ta	Cu	Al	Ta	Cu	Al	Ta	Cu	Al	Ta
CAT1												
mass%	83.12	11.55	5.33	84.69	10.28	5.03	49.42	6.30	44.28	32.48	4.02	63.49
at%	74.09	24.24	1.67	74.75	23.28	1.97	61.92	18.60	19.48	50.55	14.75	34.70
CAT2												
mass%	85.15	9.37	5.47	84.89	9.20	5.90	–	–	–	19.54	1.59	78.87
at%	78.01	20.23	1.76	78.14	19.95	1.91	–	–	–	38.32	7.35	54.32
CAT3												
mass%	84.27	9.11	6.62	85.52	9.15	5.33	19.92	5.56	74.53	24.32	2.11	73.58
at%	77.98	19.86	2.15	78.49	19.79	1.72	33.65	22.12	44.23	44.12	9.0	46.88
CAT4												
mass%	84.49	10.30	5.20	83.83	10.51	5.66	17.14	6.88	75.98	11.97	0.50	87.53
at%	76.40	21.95	1.65	75.82	22.38	1.80	28.55	26.99	44.46	27.28	2.67	70.05

high-temperature deformation defects are reduced by decreasing Al/Ta ratio in CuAlTa alloys. As given in Table 3, the required activation energy (E_0) for oxidation is increased with increasing Ta element. This result is desirable for high-temperature shape-memory alloys (Fig. 5).

The microstructure of Cu–Al–Ta HTSMA's samples was studied by optical microscope with 2000 × magnification. The result of optical microscope is shown in Fig. 7. In the optical micrographs of all samples, the dominant β'_1 (18R)-type martensite and small fine γ'_1 (2H)-type martensite were observed [9]. V-type and lath-type (needle) martensite plates were seen outside the CAT2 sample. The OM of the CAT2 alloy did not show any martensite plates because, in the sudden cooling, α (Cu)-rich precipitation phases were formed in the martensitic phase. These martensite plates are confirmed by analysis of XRD. The presence of some precipitates was found alongside the martensite plates. Figure 6e–h in the SEM photographs shows that the white and gray phases precipitate. The amount of Ta₂(Al,Cu)₃ and Cu(Al,Ta) precipitates was increased by increasing the value of Ta element. These precipitates were determined by the results of the EDX-analysis given in Table 4. However, Fig. 6f represents the high-magnification SEM images that clearly show the martensite plates.

The X-ray diffraction patterns of alloys are shown in Fig. 7. The diffraction peaks of the martensite (β'_1, γ'_1), precipitates [Ta₂(Al₂Cu₃) and Cu(Al₂Ta)] and decompositions (β_1) can be observed in all samples. In particular, in CAT3 and CAT4 alloys, the peak intensity of precipitation and decomposition decreased when Ta content increased.

The micro-hardness tests were performed for different ratios of Al/Ta element. Five different regions have been

**Fig. 7** X-ray diffraction patterns of CuAlTa alloys at room temperature

chosen to test by exerting 100 g of load for 10 s. When Silva et al. [38] added Ag and Mn elements to CuAl-based alloys, they found that the micro-hardness values of the alloys were between 230 and 310 HV. The obtained micro-hardness values for CAT1, CAT2, CAT3 and CAT4 were 295, 305, 296 and 300 HV, respectively. These results show that the micro-hardness values were increased with the addition of Ta to CuAl-based alloys.

Conclusions

The results of thermal and microstructure analysis of CuAlTa alloys, with different compositions, have been summarized as the following bullet points:

- It was determined that CuAlTa alloys exhibit high-temperature shape-memory alloy properties. Furthermore, it was seen that the phase transformation temperatures were decreased as the amount of Ta increased. However, the enthalpy change of the alloys was decreased by decreasing Al/Ta ratio.
- The results of DTA curves and XRD measurements satisfied the reduction in precipitation and decomposition by increasing Ta content in the alloys.
- It was identified that CuAlTa alloys demonstrate $2H(\gamma'_1) \rightarrow DO_3(\beta_1) \rightarrow 18R(\beta'_1)$ phase transformation.
- In the results of XRD analysis, each of the γ' , β' , Cu_9Al_4 , $CuAl$ and Ta_2Al_3 phases was determined in CuAlTa HTSMAs.
- The presence of martensite plates, precipitation and decomposition were observed in the optical microscope and SEM photographs.
- It has been observed that micro-hardness values have changed due to decrease in the precipitation and decomposition with increasing Ta ratio in alloys.

Acknowledgements This work is supported by Firat University Research Project Unit under Project No FF. 16.41.

References

1. Addington M, Schodek D. Smart materials and technologies in architecture: for the architecture and design professions. London: Routledge; 2012.
2. Dagdelen F, et al. Influence of Ni addition and heat treatment on phase transformation temperatures and microstructures of a ternary CuAlCr alloy. *Eur Phys J Plus*. 2019;134(2):66.
3. Qader IN, Kök M, Dağdelen F. Effect of heat treatment on thermodynamics parameters, crystal and microstructure of (Cu–Al–Ni–Hf) shape memory alloy. *Phys B Condens Matter*. 2019;553:1–5.
4. Kajiwara S. Characteristic features of shape memory effect and related transformation behavior in Fe-based alloys. *Mater Sci Eng, A*. 1999;273:67–88.
5. Alaneme KK, Okotete EA. Reconciling viability and cost-effective shape memory alloy options—a review of copper and iron based shape memory metallic systems. *Eng Sci Technol Int J*. 2016;19(3):1582–92.
6. Melton K. Ni–Ti based shape memory alloys. *Eng Asp Shape Mem Alloys*. 1990;344:21–5.
7. L'excellent C. Shape-memory alloys handbook. New York: Wiley; 2013.
8. Tang S, Chung C, Liu W. Preparation of CuAlNi-based shape memory alloys by mechanical alloying and powder metallurgy method. *J Mater Process Technol*. 1997;63(1–3):307–12.
9. Wang C, et al. A new type of Cu–Al–Ta shape memory alloy with high martensitic transformation temperature. *Smart Mater Struct*. 2013;23(2):025018.
10. Manzoni A, et al. Shape recovery in high temperature shape memory alloys based on the Ru–Nb and Ru–Ta systems. In: European symposium on martensitic transformations. EDP Sciences. 2009.
11. Van Humbeeck J, Stalmans R. Shape memory alloys, types and functionalities. In: Encyclopedia of smart materials. 2002.
12. Miura S, Morita Y, Nakanishi N. Superelasticity and shape memory effect in Cu–Sn alloys. In: Shape memory effects in alloys. Berlin: Springer; 1975. p. 389–405.
13. Ahlers M. Martensite and equilibrium phases in Cu–Zn and Cu–Zn–Al alloys. *Prog Mater Sci*. 1986;30(3):135–86.
14. Perkins J. Shape memory effects in alloys. Berlin: Springer; 2012.
15. Duerig TW, Melton K, Stöckel D. Engineering aspects of shape memory alloys. London: Butterworth-Heinemann; 2013.
16. Duerig TW, Albrecht J, Gessinger GH. A shape-memory alloy for high-temperature applications. *JOM*. 1982;34(12):14–20.
17. Sutou Y, et al. Characteristics of Cu–Al–Mn-based shape memory alloys and their applications. *Mater Sci Eng, A*. 2004;378(1):278–82.
18. Raju T, Sampath V. Influence of aluminium and iron contents on the transformation temperatures of Cu–Al–Fe shape memory alloys. *Trans Indian Inst Met*. 2011;64(1–2):165.
19. Schick JR, Hartl DJ, Lagoudas DC. Incorporation of shape memory alloy actuators into morphing aerostructures. In: Morphing aerospace vehicles and structures. 2012. p. 231–260.
20. Ionaitis R, Kotov V, Shchukin I. Application of shape-memory alloys in nuclear power. *At Energy*. 1995;79(4):712–4.
21. Hartl DJ, Lagoudas DC. Aerospace applications of shape memory alloys. *Proc Inst Mech Eng Part G J Aerosp Eng*. 2007;221(4):535–52.
22. Adorno A, Silva R. Effect of Ag additions on the reverse martensitic transformation in the Cu–10 mass% Al alloy. *J Therm Anal Calorim*. 2006;83(1):241–6.
23. Tadaki T. Cu-based shape memory alloys. In: Shape memory materials. 1998. p. 97–116.
24. Yang S, et al. Microstructure characterization, stress–strain behavior, superelasticity and shape memory effect of Cu–Al–Mn–Cr shape memory alloys. *J Mater Sci*. 2017;52(10):5917–27.
25. Cenoz I, Gutierrez M. Phase transformations in Cu–Al alloy. *Met Sci Heat Treat*. 2011;53(5–6):265–9.
26. Aydoğdu Y, et al. Thermal properties, microstructure and microhardness of Cu–Al–Co shape memory alloy system. *Trans Indian Inst Met*. 2014;67(4):595–600.
27. Silva R, et al. Characteristics of the Cu–18.84 at.% Al–10.28 at.% Mn–1.57 at.% Ag alloy after slow cooling from high temperatures. *J Therm Anal Calorim*. 2015;121(3):1233–8.
28. Salzbrenner R, Cohen M. On the thermodynamics of thermoelastic martensitic transformations. *Acta Metall*. 1979;27(5):739–48.
29. Kök M, Aydoğdu Y. Effect of composition on the thermal behavior of NiMnGa alloys. *J Therm Anal Calorim*. 2013;113(2):859–63.
30. Malkoc T, Dagdelen F. Production of CoAl and CoAlCr FSMAs and determination of their thermal, microstructure, and magnetic properties. *J Therm Anal Calorim*. 2019;135:1–6.
31. Yıldız K, Kök M, Dağdelen F. Cobalt addition effects on martensitic transformation and microstructural properties of high-temperature Cu–Al–Fe shape-memory alloys. *J Therm Anal Calorim*. 2015;120(2):1227–32.
32. Kwarciak J, Bojarski Z, Morawiec H. Phase transformation in martensite of Cu–12.4% Al. *J Mater Sci*. 1986;21(3):788–92.

33. Liu X, et al. Phase equilibria in the Cu-rich portion of the Cu–Al binary system. *J Alloys Compd.* 1998;264(1–2):201–8.
34. Prashantha S, Mallikarjun U, Shashidhara S. Effect of ageing on shape memory effect and transformation temperature on Cu–Al–Be shape memory alloy. *Procedia Mater Sci.* 2014;5:567–74.
35. Soliman H, Habib N. Effect of ageing treatment on hardness of Cu–12.5 wt% Al shape memory alloy. *Indian J Phys.* 2014;88(8):803–12.
36. Dagdelen F, Ercan E. The surface oxidation behavior of Ni–45.16%Ti shape memory alloys at different temperatures. *J Therm Anal Calorim.* 2014;115(1):561–5.
37. Saud SN, et al. Effect of Ta additions on the microstructure, damping, and shape memory behaviour of prealloyed Cu–Al–Ni shape memory alloys. *Scanning.* 2017. <https://doi.org/10.1155/2017/1789454>.
38. Silva R, et al. Investigation of thermal, mechanical and magnetic behaviors of the Cu–11% Al alloy with Ag and Mn additions. *Mater Character.* 2013;75:194–9.

Publisher's Note Springer Nature remains neutral with regard to jurisdictional claims in published maps and institutional affiliations.